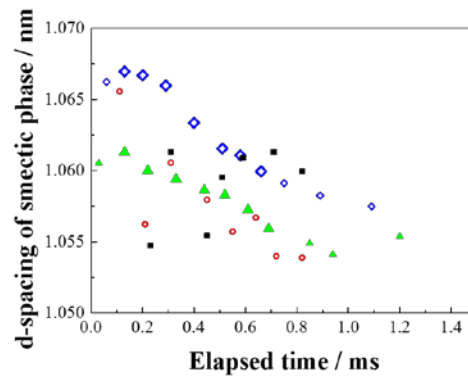
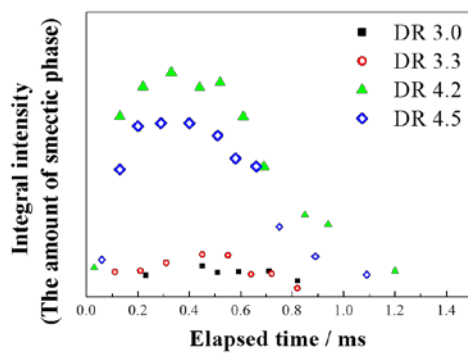


Highlights

- Draw ratio dependence of fiber structure development was analyzed by WAXD/SAXS.
- No smectic phase, but an X-pattern, was observed at minimum draw ratio.
- The amount of smectic phase increased with drawing stress up to 100 MPa.
- The smectic phase d -spacing increased with drawing stress over 100 MPa.
- Tensile strength of drawn fiber increased with smectic phase amount and d -spacing.

Graphical abstract



Effect of draw ratio on fiber structure development of polyethylene terephthalate

R. Tomisawa^a, T. Ikaga^a, K. H. Kim^a, Y. Okoshi^{a,b}, K. Okada^c,
H. Masunaga^d, T. Kanaya^e, M. Masuda^f, and Y. Maeda^f

^a*Faculty of Textile Science and Technology, Shinshu University, 3-15-1 Tokida, Ueda, Nagano 386-8567, Japan.*

^b*Institute for Fiber Engineering, Shinshu University Tokida 3-15-1, Ueda, Nagano 386-8567, Japan.*

^c*Material Science Laboratories, Toray Research Center, 3-3-7 Sonoyama, Otsu, Shiga 520-8567, Japan.*

^d*Japan Synchrotron Radiation Research Institute, 1-1-1 Kouto, Sayo-cho, Hyogo 679-5148, Japan*

^e*High Energy Accelerator Research Organization, 203-1 Shirakata, Tokai, Ibaraki 319-1106, Japan.*

^f*Fibers and Textiles Research Laboratories, Toray, 4845 Mishima, Shizuoka 411-8652, Japan.*

*Corresponding author. *E-mail address:* yokoshi@shinshu-u.ac.jp (Y. Okoshi)

Abstract

Fiber properties are decided by its structure, and the structure are mainly formed in the fiber drawing process. In this study, the effects of the draw ratio on the fiber structure development of polyethylene terephthalate after continuous neck-drawing were investigated using simultaneous WAXD/SAXS measurements. Low-oriented amorphous as-spun fibers were drawn to a draw ratio of 3.0–4.5, at which the fiber can be stably neck drawn. WAXD and SAXS images were obtained up to 2.0 ms when the structure was mainly developed. The smectic (001') diffraction intensity and long period increased with increasing draw ratio up to 4.2, and a larger (001') diffraction *d*-spacing was observed at a draw ratio of 4.5. The results suggest that more fibrillar structures were formed with increasing draw ratio up to 4.2, and more constrained molecular bundles were formed at a draw ratio of 4.5. A larger amount of constrained fibrillar structures can bear a greater tensile force in tensile tests, therefore the drawn fibers have higher tensile strengths.

Keywords: polyethylene terephthalate, WAXD/SAXS, smectic phase

1. Introduction

Polyethylene terephthalate (PET) was first synthesized by Whinfield and Dickson in 1941 [1]. PET fibers are now the most produced synthetic fiber, and because they are commonly used in industry, improvements in their strength are desirable. There have been a huge number of studies of the relationship between the structure and properties of PET fibers, particularly focusing on improvement of their strength. In general, a higher molecular orientation and higher crystallinity increase the strength of synthetic fibers. However, in the case of highly oriented fibers, although the strength increases more with increasing draw ratio, the molecular orientation and crystallinity tend to reach a maximum value. The improved strength is explained by the increase in taut tie chains connecting the crystallites in the microfibrils [2, 3]. Other fiber properties, Young's modulus and thermal shrinking behavior, for example, are also explained by the higher-order structure, i.e., taut tie chains and microfibrils. However, it is difficult to evaluate the higher-order structures quantitatively by structural analysis of a drawn fiber. Therefore, new information on the higher-order structures of PET fibers is needed for designing and evaluating the fiber properties.

To obtain new information on the higher-ordered structures of synthetic fibers, the orientation-induced crystallization of polymeric materials has been investigated by in situ X-ray studies of fiber structure development. For example, Haberkorn et al. [4] obtained X-ray images of a polyamide 66 high-speed spin-line. They observed the structure development at a time resolution of 0.16 ms, using a fiber running speed of 5500 m/min and a necking width fluctuation of about 3 cm. Kolb et al. [5] obtained X-ray images of PET on a 4000 m/min high-speed spin-line with a time resolution of ± 0.3 ms. X-ray studies of the batch drawing process have also been performed; for example, Mahendrasingam et al. [6] and Kawakami et al. [7] observed strain-induced phase-transition phenomena of PET films. In situ studies of the continuous drawing process have also been performed. Ran et al. [8] and Wu et al. [9] reported the draw ratio dependence of fiber structure development based on in situ examination of a pin drawing process. However, because fiber structure development in a continuous drawing process is completed within a few milliseconds, it was difficult to monitor the fiber structure development precisely.

It has been suggested that laser-heated drawing would overcome this difficulty. Because the necking point is located in the laser beam by rapid and homogeneous heating with laser irradiation, changes in diameter [10], temperature [11], and structure after necking can be measured precisely. The temperature profile of the process agreed well with the temperature profile predicted using energy balance equations [12]. Wide-angle X-ray diffraction (WAXD) and small-angle X-ray scattering (SAXS) patterns were also obtained by using a combination of laser-drawing and an ultrahigh-intensity X-ray source of synchrotron radiation, and they were used to investigate fiber structure

development after necking for PET [13–15], poly(ethylene naphthalate) [16], polypropylene [17], poly(phenylene sulfide) [18], poly(butylene terephthalate) [19], and sea–island conjugated Polystyrene/PET [20]. Particularly, Yamaguchi et al. investigated the structure development of PET fibers drawn to various draw ratios similarly to this work. However, no clear draw ratio dependence of the structure development was observed, possibly because the time resolution of the measurements was insufficient. In contrast, Sugawara et al. [20] also reported a draw ratio dependence at a time resolution of 0.09–0.12 ms. They found that a larger amount of the smectic phase was formed at higher draw ratios. However, they compared only two sets of draw ratio conditions, and this is insufficient for analyzing the relationship between fiber structure development and the mechanical properties of a drawn fiber. Therefore, in this study, we examined the relationship in detail, focusing on the changes of stress-bearing structure at higher draw ratios. Specifically, we tried to explain the draw ratio dependence of the tensile strength and thermal shrinkage stress by the changes in structural parameters with the fiber structure development, i.e., the amount and d -spacing of the smectic (001') diffraction, and the long period obtained by the SAXS images.

2. Experimental

2.1 Sample

The fibers used for drawing were prepared by melt-spinning PET ($IV = 1.3$ dL/g) provided by the Toray Co. The polymer was heated at 310 °C, extruded from a one-hole nozzle at a mass flow rate of 4.8 g/min, and taken-up at 500 m/min. The nozzle diameter was 1.0 mm, and the length/diameter ratio was 3.

2.2 Drawing

The drawing system used has been described in a previous report [13]. Fibers were fed continuously from a feed roller, heated by irradiation with a CO₂ laser beam, and drawn based on the speed difference between the feed and take-up rollers. The fiber running speed after necking was fixed at 110 m/min, and the draw ratio was changed by changing the fiber-feeding speed. A random polarized laser beam of wavelength and diameter 10.6 μm and 6 mm, respectively, was generated using a PIN-30R laser (Onizuka Glass Co., Ltd.). The beam was used to irradiate running fibers from three different directions. The drawing tension was measured using a tension meter (HS-1500S, Eiko Sokki Co., Ltd.) A 100 gf pickup was installed between the neck-drawing point and the take-up roller. The drawing stress was calculated from the drawing tension and the diameter of the drawn fiber. The drawing conditions are shown in Table 1. The range of draw ratios, 3.0–4.5, was the range for stable neck-drawing during more than 5 min, i.e., the neck-drawing point was not stable at a draw ratio less than 3.0, and the fiber was liable to break at a draw ratio above 4.5. The minimum draw ratio of 3.0 was almost equal to the natural draw ratio (NDR) estimated from the stress–strain curve for the as-spun

fibers. The laser power for each drawing condition was determined to enable fluctuations in the neck-drawing point to be minimized.

2.3 On-line measurements

The on-line measurement system has been described in a previous report [13]. WAXD/SAXS patterns were obtained by X-ray irradiation of the running fiber. The X-ray beam size was 40 μm vertically and 50 μm horizontally. The distance from the necking point to the X-ray irradiation position was changed by moving the laser irradiation position. The elapsed time after necking was calculated by dividing the distance by the fiber running speed.

The synchrotron X-ray beam used in this study was provided by SPring-8 BL03XU (FSBL), with an undulator to give an ultrahigh-intensity X-ray beam. The X-ray wavelength was 0.10 nm. The camera lengths for the WAXD and SAXS measurements were 78.7 and 1788 mm, respectively, the exposure times were 1 and 50 s, respectively, and the detectors used for each measurement were a 1032 \times 1032 pixel flat panel detector (50 μm /pixel) and a 672 \times 512 pixel charge-coupled device (126 μm /pixel), respectively. After subtraction of air scattering, the obtained image was normalized by the total integrated intensity to compensate for fluctuations in the X-ray irradiation volume.

The position resolution was calculated from the fluctuations of the necking point, i.e., 0.09–0.14 mm, the width of the necking point, i.e., 0.13–0.28 mm, and the width of the X-ray beam, i.e., 0.05 mm. The average position of the necking point and its fluctuation were determined by analysis of still images taken from the video movie recorded during the measurements. The resolution time was calculated using a previously reported method [20]. The obtained time resolution was 0.09–0.16 ms.

2.4 Birefringence

The birefringence of the drawn fiber was measured using a polarizing microscope (BX51-33POC, Olympus Co., Ltd.) with a 546 nm monochromatic filter. Tricresyl phosphate was used as the immersion oil. The birefringence average and standard deviation were calculated for every 10 samples.

2.5 Thermomechanical tests

The thermal and mechanical properties of the drawn fibers were investigated using tensile tests, thermomechanical analysis, and differential scanning calorimetry (DSC). The strength, elongation, Young's modulus, and NDR were measured using an Autograph AGS-X instrument (Shimadzu Co., Ltd.) equipped with a 50 N load cell and air chuck. The sample length and elongation rate were 40 mm and 100%/min, respectively, and the average and standard deviation were calculated for every 10 samples. The NDR was defined as the draw ratio at which the tensile stress began to increase again with dissipation of the necking point.

A thermomechanical analyzer (TMA/SS6100, SII Nanotechnology Inc.) was used to determine

the thermal shrinkage factor and shrinkage stress at heating rates of 5 and 10 K/min, respectively. The sample length was 10 mm in both cases. A Thermoplus DSC8230 instrument (Rigaku Co., Ltd.) was used for DSC analysis at a heating rate of 10 K/min. A powdery cut fiber sample was used for the measurements.

3. Results and discussion

3.1 Structure and properties of drawn fibers

The structure and properties of the drawn fibers are listed in Tables 1 and 2. The crystallinity was determined using DSC, based on a heat of fusion of 135 kJ/kg [21]. The birefringence and crystallinity of the drawn fibers increased with increasing draw ratio but seemed to reach a maximum value at a draw ratio above 4.2. The properties of the drawn fibers also changed with changes in the draw ratio; the tensile strength, Young's modulus, thermal shrinkage factor, maximum thermal shrinkage stress, and temperature of maximum shrinkage increased, whereas the elongation decreased, with increasing draw ratio. However, there were some differences at draw ratios greater than 4.2. The Young's modulus and shrinkage factor seemed to reach a maximum value above a draw ratio of 4.2, whereas the tensile strength, elongation, and shrinkage stress continue to change. These results indicate that the effect of draw ratio on the fiber structure changed at a draw ratio of 4.2. We therefore focused on the difference between the draw ratio dependence of the fiber structure development at draw ratios below and above 4.2.

Table 1 Drawing conditions and structural parameters of drawn fibers.

Draw ratio	Laser power /W	Drawing stress / MPa	Birefringence $\times 10^3$	Crystallinity / %
as-spun	-	-	4	12
3.0	18	22	118	27
3.3	19	29	151	34
4.2	22	103	182	42
4.5	25	149	198	38

Table 2 Mechanical and thermomechanical properties of drawn fibers.

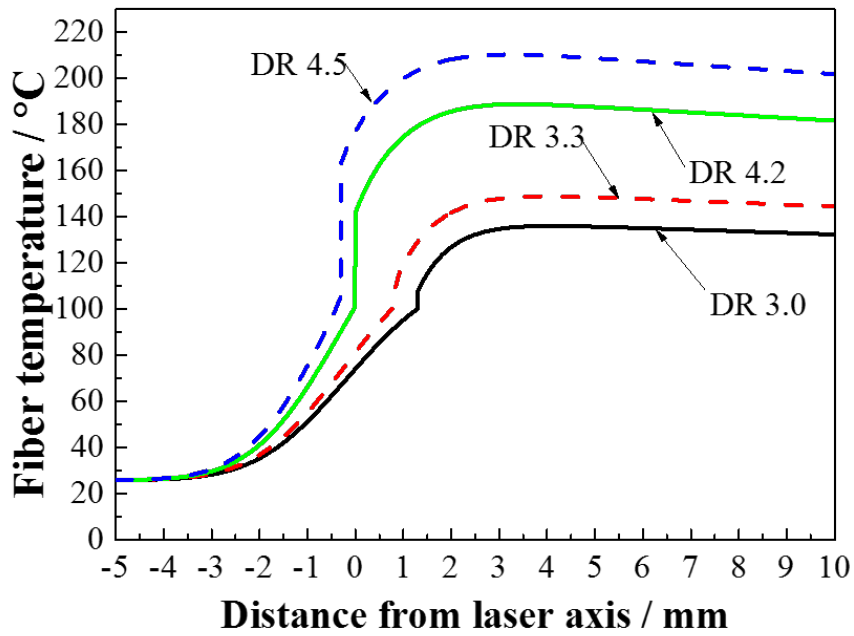
Draw ratio	Young's modulus / GPa	Tensile strength / MPa	Elongation / %	Shrinkage at 200°C / %	Maximum shrinkage stress	
					Stress / MPa	Temperature / %
as-spun	2.2	175	616	-	-	-
3.0	7.6	582	95	5	17	101
3.3	9.4	629	69	7	30	117
4.2	12.6	916	38	9	72	180
4.5	12.3	1030	27	8	78	194

3.2 Fiber temperature profiles

The fiber temperature profile around the neck-drawing point was determined using a forward difference method, based on the energy balance equation, with consideration of the laser irradiation energy, heat transfer from the fiber surface, work of plastic deformation by an external force, and latent heat of crystallization [11]. The absorption coefficient of PET, $1.149 \times 10^4 \text{ m}^{-1}$, obtained for the laser beam wavelength was used to calculate the laser irradiation energy [11]. The heat transfer coefficient was estimated experimentally using the equation proposed by Kase and Matsuo [22]. The heat of crystallization and the heat of fusion of the drawn fibers were determined using DSC.

Figure 1(a) shows plots of the estimated fiber temperature against the distance from the laser beam axis. The fiber temperature began to rise at -3 mm , when the laser beam began to irradiate the fibers. Fiber necking occurred when the fiber temperature was near the glass-transition temperature. The fiber temperature increased steeply as a result of the heat of plastic deformation at the necking, continued to increase by the heat of laser irradiation and the latent heat of crystallization, and reached a maximum at the edge of the laser beam ($+3 \text{ mm}$). The fiber temperature then decreased to room temperature by heat transfer. Necking occurred at almost the same temperature for all draw ratios. This is because the increase in the laser power and the decrease in the fiber running speed before necking are cancelled by the upstream shift of the necking. In contrast, the steep increase in the fiber temperature at necking increased with increasing draw ratio because of the increase in applied work at necking. The maximum fiber temperature also increased with increasing draw ratio. In particular, for a draw ratio from 4.2 to 4.5, in spite of the small difference in the draw ratio, the temperature increased greatly because of the large increase in the drawing stress. In Figure 1(b), the horizontal axis is converted to elapsed time after necking. As discussed below, the fiber structure mainly developed in the 2 ms after necking. The temperatures at 0 and 2 ms after necking are shown in Table 3.

(a)



(b)

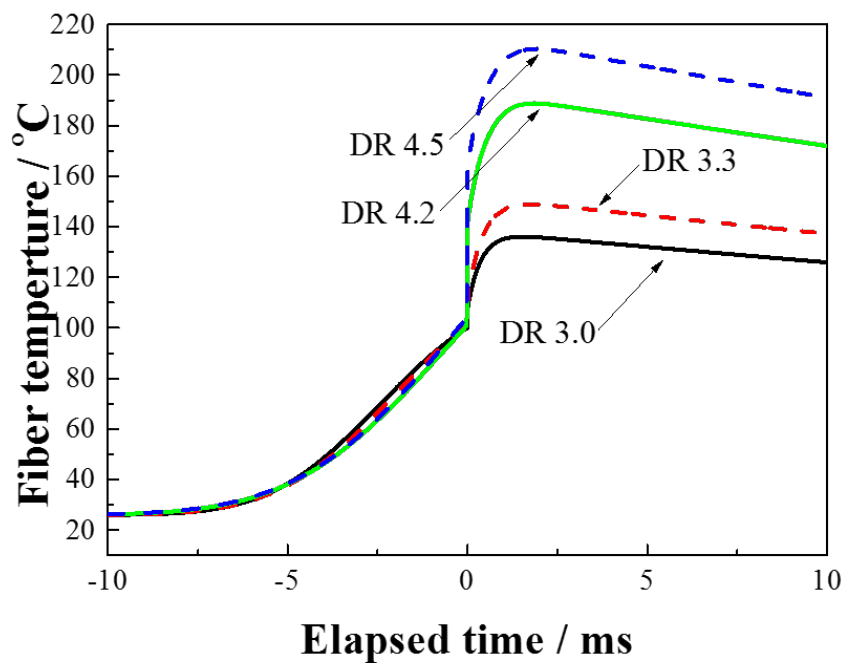


Figure 1 Estimated fiber temperatures plotted against (a) elapsed time after necking and (b) distance against necking point. Draw ratios (DR) are shown in the figure.

3.3 WAXD image

The WAXD images are shown in Figure 2. The elapsed times after necking are noted in the figure. In particular, for a higher draw ratio, a sharp meridional diffraction with a long streak along the layer line was observed at around 0.3 ms after necking. This is the (001') diffraction of the smectic phase, which is a metastable structure formed during batch drawing [7] or heat-treatment of an oriented amorphous material [23]. The smectic phase was first reported by Bonart [24], and has also been reported for poly(ethylene naphthalate) [16] and poly(butylene terephthalate) [25]. After 0.5 ms, the intensity of the (001') diffraction started to decrease and an equatorial broad peak separated into the (010), (-110), and (100) crystal diffractions. The stronger and sharper equatorial diffractions observed for the fibers drawn 4.2 and 4.5 times than for those drawn 3.0 and 3.3 times suggest a higher crystallinity and higher crystal orientation of the former than of the latter. However, there were no clear differences between the crystallinities and crystal orientations observed for the fiber drawn 4.2 times and that drawn 4.5 times.

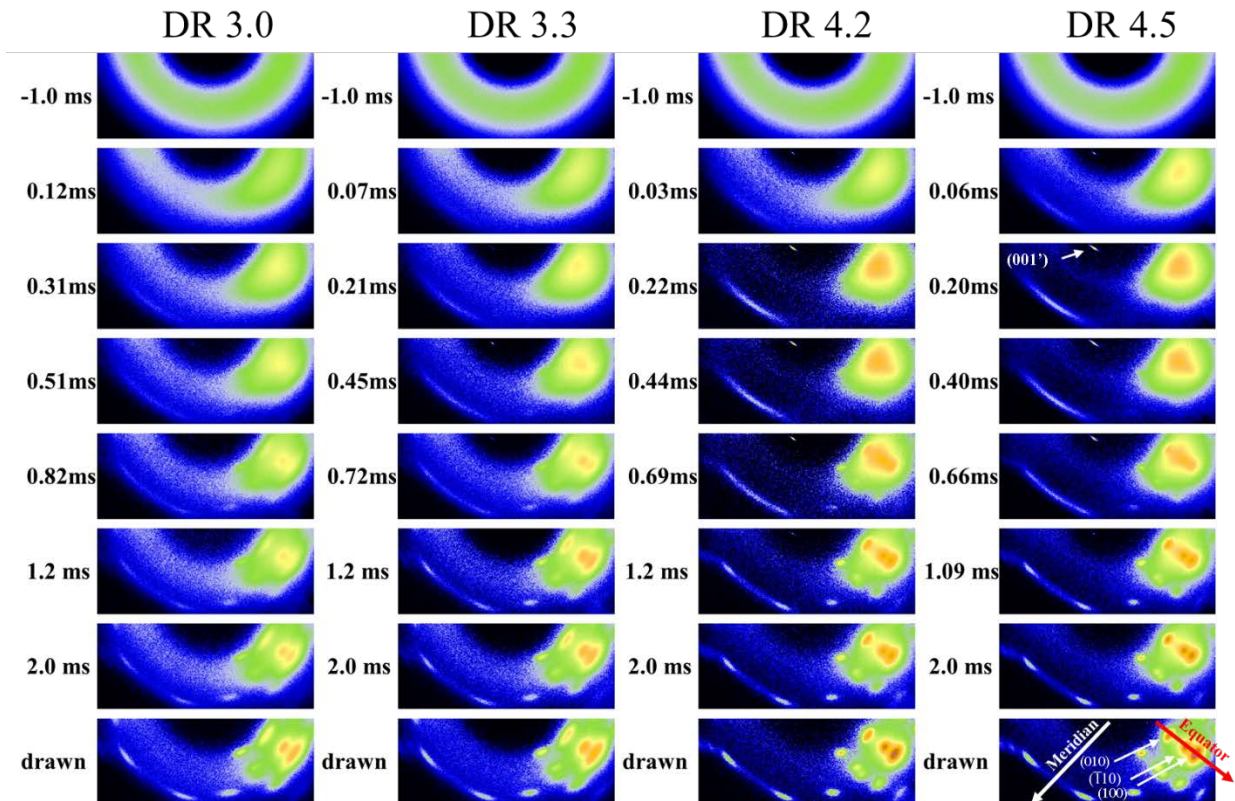


Figure 2 Wide-angle X-ray diffraction patterns at corresponding elapsed times after necking. Draw ratios (DR) are shown.

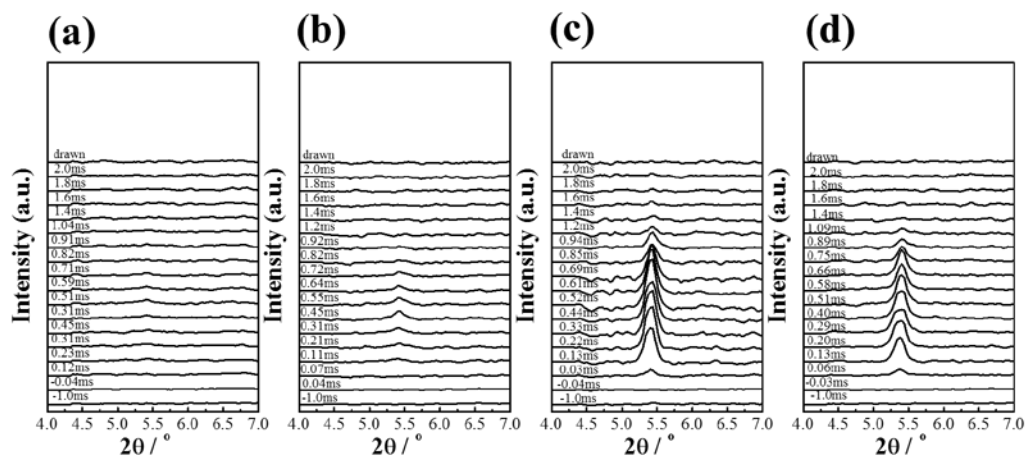


Figure 3 Meridional X-ray intensity profiles at draw ratios (a) DR 3.0, (b) DR 3.3, (c) DR 4.2, and (d) DR 4.5.

3.4 Smectic phase

The meridional intensity profiles obtained from Figure 2 are shown in Figure 3. A sharp smectic (001') diffraction was observed at a diffraction angle of 5.4° . The integral intensity and the d -spacing calculated using the Bragg equation are shown in Figures 4 and 5, respectively. The intensity reached a maximum at about 0.3 ms, and then decreased. The intensity clearly increased with increasing draw ratio from 3.0 to 4.2, and the diffraction could be observed for a longer time after necking. In contrast, the intensity did not increase but the d -spacing increased with increasing draw ratio from 4.2 to 4.5. Because the d -spacing for a draw ratio of 4.5 was close to the length of the chemical repeating unit, 1.077 nm [26], the smectic phase seems to be composed of almost fully extended chains. The larger d -spacing is caused by the higher drawing stress applied to the smectic phase. A larger stress is also applied to the molecular network including the smectic phases, and extends the molecular chains connecting the smectic phases.

Yamaguchi et al. reported that the d -spacing increases with increasing draw ratio, but no clear dependence of the intensity on the draw ratio was reported [13]. This phenomenon could be explained by the insufficient time resolution of the measurements. Because of the restriction of their light source generated by a bending magnet system, the time resolution of their measurements was no less than 0.6 ms. The light source generated by the undulator-equipped system used in this study had an intensity 10^4 times that of a bending magnet system [27]. It gave a shorter resolution time of about 0.1 ms and images with improved signal/noise ratios, which enabled a more quantitative evaluation of the draw ratio dependence of the (001') intensity. Sugawara et al. also used an undulator-equipped system and reported that the intensity increased with increasing draw ratio, but there was no obvious change in the d -spacing [20]. The results of this work suggest that an increase in the d -spacing is only observed at high draw ratios, at which the amount of smectic phase is saturated.

A clear decreasing trend in the d -spacing was also observed for a draw ratio of 4.5. Kawakami et al. [7] reported the increase of d -spacing before the phase transition from smectic phase to crystal. The opposite tendency is caused by the difference of drawing conditions, i. e. batch drawing and continuous drawing. For batch drawing, smectic phase was formed with the increase of molecular orientation. While for continuous drawing in this study, it was formed after necking. The d -spacing decrease is accompanied by emission of stored energy. Kim et al. [14] observed the delayed emission of stored energy 0.6 ms after necking by measuring the fiber temperature profiles, i.e., part of work of the external force applied at the necking is stored elastically in the smectic phase, and emitted by the relaxation that is indicated by the d -spacing shrinkage. The relaxation is accompanied by transformation of the smectic phase to the triclinic crystal.

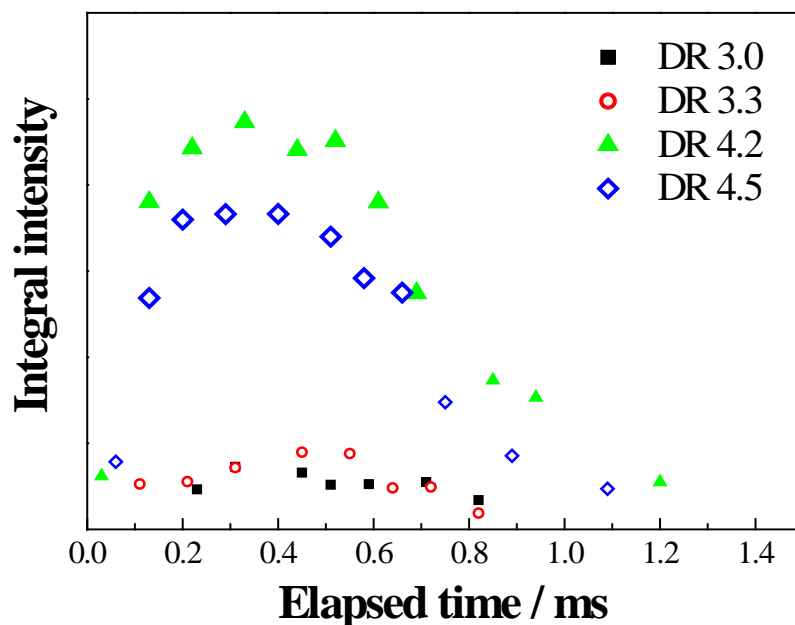


Figure 4 Integrated intensities of smectic (001') diffractions plotted against elapsed time after necking. Draw ratios (DR) are shown in figure. Small plots indicate lower diffraction intensities and are less reliable.

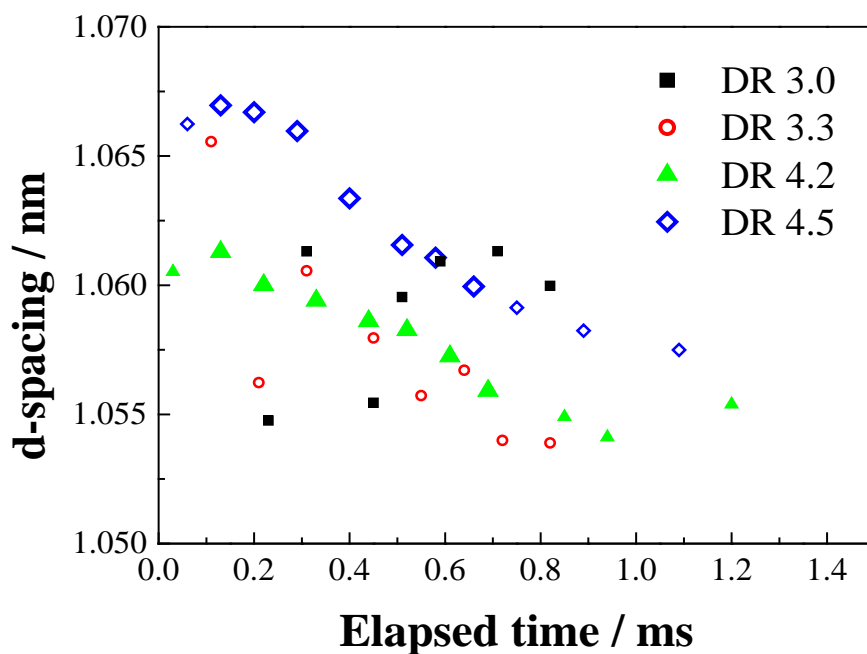


Figure 5 Plots of (001') diffraction d -spacings against elapsed time after necking. Draw ratios (DR) are shown in figure. Small plots indicate lower diffraction intensities, as in Figure 4.

3.5 Crystallization

The intensity profiles along the equatorial direction obtained from Figure 2 were fitted to a Gaussian curve (equation 1); $2\theta_0$, I_0 , and β are the position, intensity, and full width at half maximum, respectively, of the peak.

$$I(\theta) = I_0 \exp \left\{ -4 \ln 2 \times \left(\frac{2\theta - 2\theta_0}{\beta} \right)^2 \right\} \quad (1)$$

The equatorial intensity profiles can be well separated into (010), (-110), and (100) crystal diffractions, and broad peaks from amorphous or smectic phases. The crystallinity index was determined from the fraction of the integrated intensity of the crystal diffractions with respect to the total integrated intensity. The crystallinity indices for all the samples started to increase from 0.5 ms after necking, and were almost saturated at 2.0 ms (Figure 6). However, because they are clearly lower than those of drawn fibers, secondary crystallization should be occurred after 2.0 ms. The crystallization rate K_c , crystallization induction time t_0 , and final crystallinity $X_{c\infty}$ were estimated using equation 2, based on the crystallinity indices up to 2.0 ms after necking; the values are listed in Table 3.

$$X_{c(t)} = \left\{ 1 - K_c \exp(t - t_0) \right\} X_{c\infty} \quad (2)$$

The $X_{c\infty}$ value increased with increasing draw ratio up to 4.2, in agreement with the trend in the crystallinities of the drawn fibers. In contrast, there were no clear draw ratio dependences at crystallization rates of 2.3–2.8 ms^{-1} and crystallization induction times of 0.4–0.6 ms. Yamaguchi et al. [13] and Sugawara et al. [20] observed similar crystallization behaviors during continuous drawing of PET, and a K_c of 0.7 ms^{-1} and t_0 of 0.6 ms were reported by the former [13]. The lower crystallization rate than the result in this study should be caused by pattern smearing at an insufficient time resolution. The crystallization rates and crystallization induction times obtained in this study are more reliable because the time resolution of 0.1 ms was sufficiently shorter than the crystallization time. It is worth noting that there were no obvious differences among the crystallization rates obtained at different draw ratios in spite of the clear difference in molecular orientation. A higher molecular orientation generally caused an increase in the crystallization rate. The crystallization rate should also increase with increasing fiber temperature for the temperature range estimated at 3.2. Therefore, the almost constant crystallization rate observed in this work indicates that orientation-induced crystallization should be

suppressed at high draw ratios, probably by formation of the smectic phase. The crystallization rate seems to be reduced by the decrease in the free energy change for crystallization via a metastable smectic phase compared with that for direct crystallization from the oriented amorphous phase, i.e., crystallization seems to be suppressed by the decreased molecular mobility in the smectic phase compared with the amorphous phase.

Table 3 Crystallization behavior.

Draw Ratio	Fiber Temperature / °C		$X_{c\infty}$ / %	t_0 / ms	K_c / 10^3 s ⁻¹
	0 ms	2 ms			
3.0	108	136	37	0.5	2.8
3.3	112	157	41	0.4	2.4
4.2	142	189	45	0.6	2.3
4.5	165	210	48	0.5	2.5

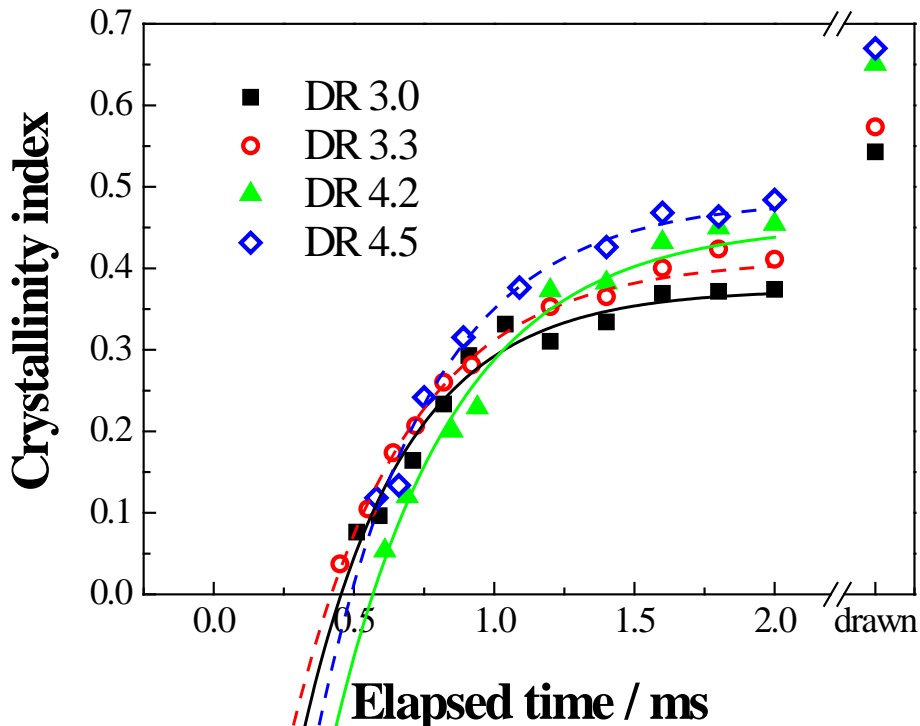


Figure 6 Crystallinity indices estimated from wide-angle X-ray diffraction equatorial profiles plotted against elapsed time after necking. Draw ratios (DR) are shown in figure.

3.6 Crystal orientation factor and tilting angle

By assuming the orientation axis of PET crystal is tilted in the (-230) plane from the c -axis [28], the tilting angle and crystal orientation factor were calculated from the intensity profile along the azimuthal angle (φ). The (010) and (100) diffractions were considered to be two overlapping peaks symmetrical to the equator, and then the intensity profiles can be expressed by equation 3. Each peak was fitted by a Pearson VII type curve, expressed by equation 4, with the peak position (φ_p) and a shape factor m of 2. The measured profiles were fitted well with the curves. The crystal orientation factor (f), i.e., the orientation factor of the orientation axis to the fiber axis, was obtained by equation 5. The tilting angle (t) was obtained from the peak positions (φ_p) and the d -spacing of (hkl) plane (d_{hkl}) using equation 6. The lattice constants used for the calculation were $a = 0.452$ nm, $b = 0.598$ nm, $c = 1.077$ nm, $\alpha = 101^\circ$, $\beta = 118^\circ$, and $\gamma = 111^\circ$, i.e., those reported by Tomashpol'skii et al. [26].

$$I(\varphi) = i(\varphi, \varphi_p) + i(\varphi, -\varphi_p) \quad (3)$$

$$i(\varphi, \varphi_p) = \frac{I_0}{\left\{ 1 + 4 \left(\frac{\varphi - \varphi_p}{\tau} \right)^2 \left(2^{\frac{1}{m}} - 1 \right) \right\}^m} \quad (4)$$

$$f = \frac{3 \langle \cos^2 \varphi \rangle - 1}{2}, \quad \langle \cos^2 \varphi \rangle = \frac{\int_0^{\pi/2} i(\varphi, 0) \cos^2 \varphi \sin \varphi d\varphi}{\int_0^{\pi/2} i(\varphi, 0) \sin \varphi d\varphi} \quad (5)$$

$$\cos \varphi_p = d_{hkl} \left[\left(\frac{h}{2} + \frac{k}{3} \right) c \sqrt{\frac{1 - \cos^2 t}{c^2 L - K^2}} + \frac{l}{c} \left(\cos t - K \sqrt{\frac{1 - \cos^2 t}{c^2 L - K^2}} \right) \right] \quad (6)$$

Where, $K = \frac{ac}{2} \cos \beta + \frac{bc}{3} \cos \alpha$, $L = \frac{a^2}{4} + \frac{b^2}{9} + \frac{ab}{3} \cos \gamma$.

The crystal orientation factors and tilting angles are shown in Figures 7 and 8, respectively. The crystal orientation factor increased, whereas the tilting angle decreased, with increasing draw ratio up to 4.2. This trend corresponds to increases in the drawing stress and birefringence. In contrast, from a draw ratio of 4.2 to 4.5, although the tilting angle continuously decreased, the crystal orientation factor was almost saturated. The saturation of the crystal orientation corresponds to that of birefringence, and the continuous decrease in the tilting angle corresponds to the increase in the smectic d -spacing, as described in section 3.4, by the increase in the drawing stress.

For draw ratios of 3.0 and 3.3, both the crystal orientation factor and tilting angle for the (100)

diffraction increased after 2 ms. The simultaneous increases in the crystal orientation factor and tilting angle suggest the formation of lamellar crystals by secondary crystallization. In contrast, for draw ratios of 4.2 and 4.5, neither the crystal orientation factor nor the tilting angle changed after 2 ms. This indicates that secondary crystallization mainly occurred in fibrils.

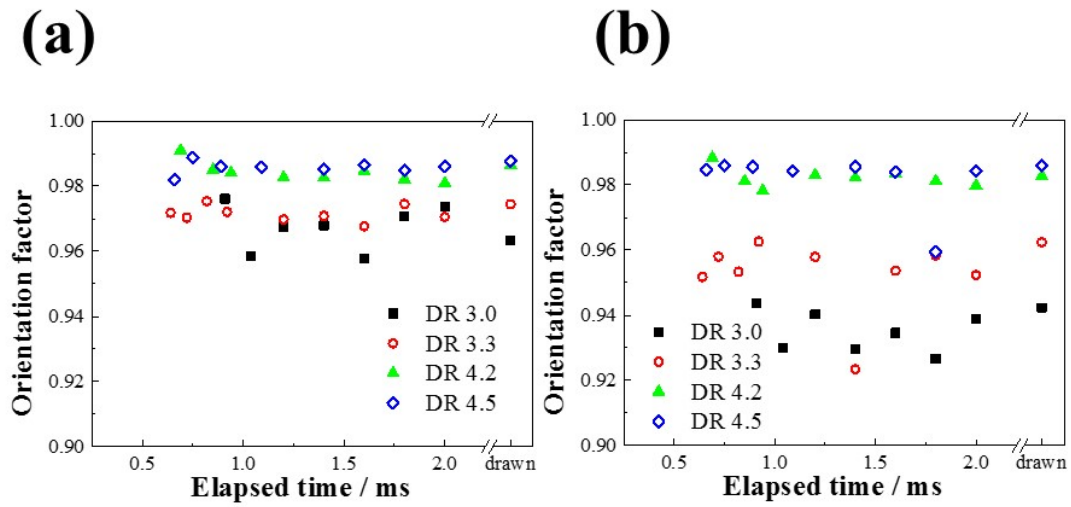


Figure 7 Orientation factors of crystal *c*-axis estimated from (a) (010) and (b) (100) diffractions plotted against elapsed time after necking. Draw ratios (DR) are shown in figure.

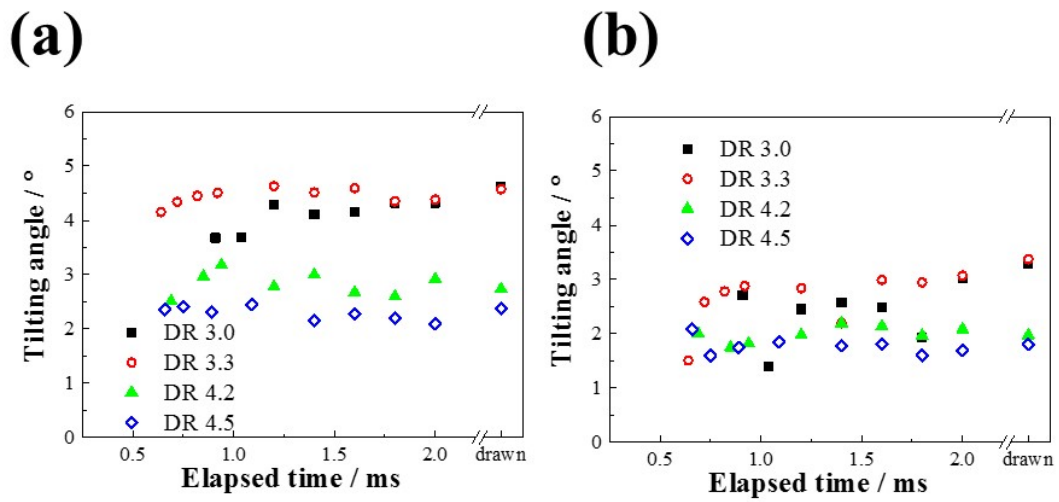


Figure 8 Tilting angles of crystal *c*-axis estimated from (a) (010) and (b) (100) diffractions plotted against elapsed time after necking. Draw ratios (DR) are shown in figure.

3.7 SAXS image

Figure 9 shows SAXS images. The scattering intensities increased with time elapsed for all draw ratios. For draw ratios of 3.0 and 3.3, the X-shaped scattering pattern observed at 0.2-0.3 ms changed to a four-point pattern 0.8 ms after necking. In contrast, for draw ratio of 4.2 and 4.5, the X-pattern was not observed, but a meridional two-point pattern overwrapped with a four-point pattern appeared directly at 0.4-0.5 ms after necking instead.

The X-patterns observed for the lower draw ratios were also observed for high-speed-spun PET fiber [29, 30]. It was explained by the series of crystallites aligned to the direction tilted to the fiber axis. Okada et al. observed changes in the SAXS image of an axial-planar-oriented PET film obtained by continuous uniaxial drawing. A two-point pattern was observed in the through-view images, whereas X-like patterns were observed in the edge-view images [31]. This suggests that the density difference along the shear-band-like structure [32] should be developed by compression along the film thickness. The shear deformation seemed to be occurred along the surface of the benzene ring because the surface oriented along the normal of film by the deformation. The X-patterns observed in this study thought to be caused by the similar shear deformation at necking. By forming crystallites along the structure, the X-pattern changed to a four-point pattern.

The peaks in the meridional intensity profiles were fitted by a Gaussian curve (equation 1), and the long periods shown in Figure 10 were calculated from the peak positions using the Bragg equation. The long periods at draw ratios of 4.2 and 4.5 were clearly higher than those at draw ratios of 3.0 and 3.3. In addition, the long periods at higher draw ratios decreased significantly up to 1.0 ms. The decrease in the long period with decreasing smectic (001') intensity suggests that the new crystallites were formed and developed in the smectic phase. This agrees with the model proposed by Yamaguchi et al. that the fibrillar smectic phase was divided into a sequence of crystallites and amorphous phases including tie molecules [13].

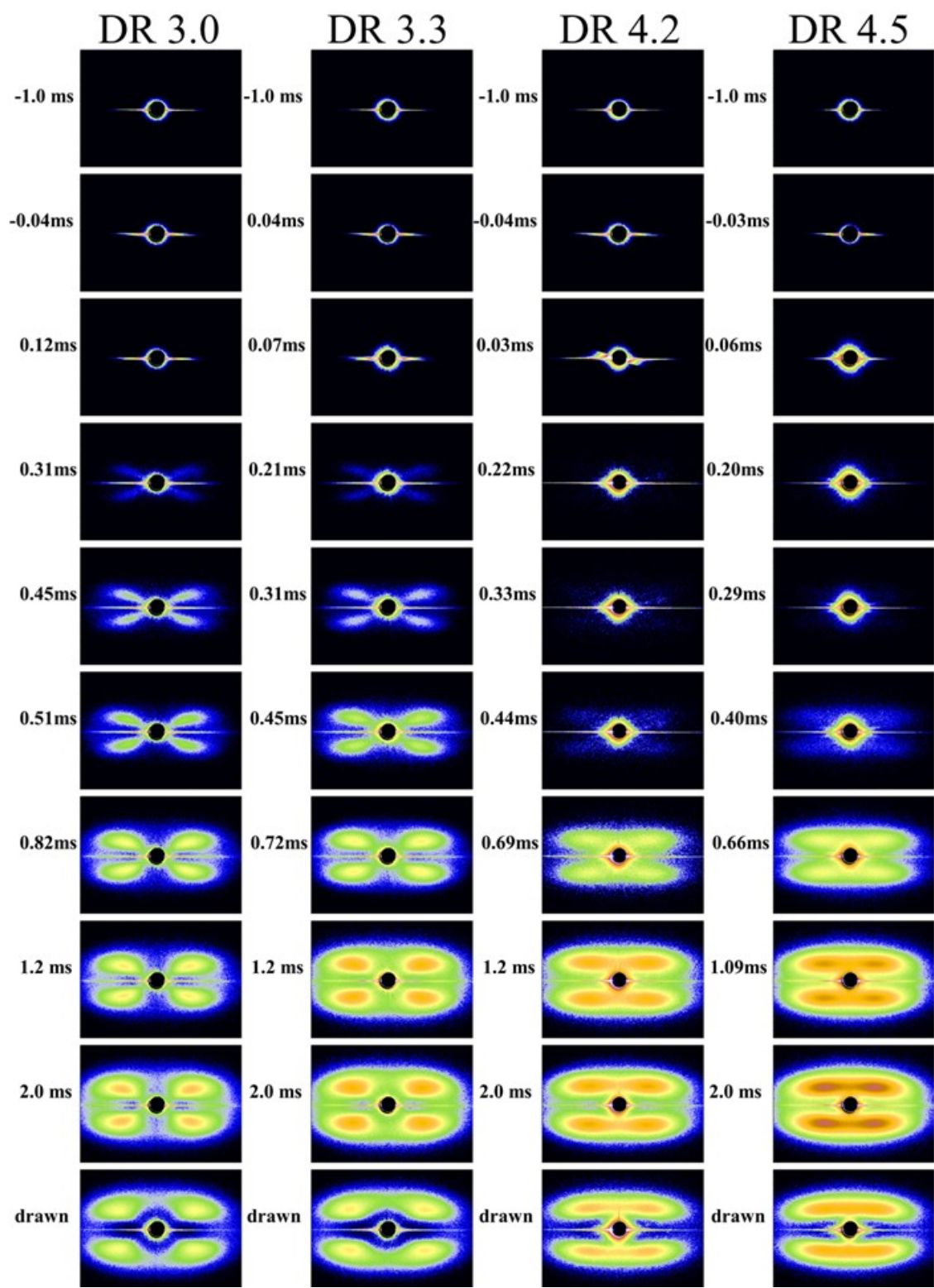


Figure 9 SAXS patterns for corresponding elapsed times after necking. Draw ratios (DR) are shown in the figure.

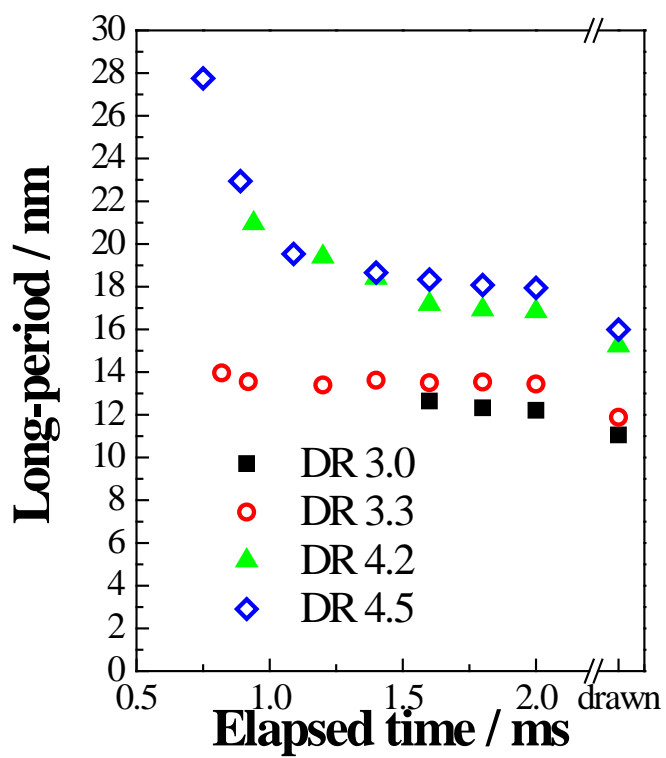


Figure 10 Long periods obtained from SAXS patterns plotted against elapsed time after necking. Draw ratios (DR) are shown in figure.

3.8 Structure development and properties of drawn fibers

Figure 11 shows a schematic diagram of fiber structure development. About 0.3 ms after necking, an X-pattern or smectic (001') diffraction appeared for lower or higher draw ratios, respectively. Both structures were transformed into structures including oriented crystallites until 2 ms, at almost the same rate. For the minimum stable draw ratio of 3.0, the X-pattern arose from shear deformation of necking, and changed to a four-point pattern until 0.8 ms after necking, with the formation of crystallites. In contrast, for draw ratios of 4.2–4.5, bundles of oriented molecular chains formed by necking were transformed into a smectic phase until 0.3 ms after necking, and further transformed into the long-period structure of crystallites and amorphous phase. The transformation from the smectic phase to the long period structure started before 0.8 ms, and almost finished at 2.0 ms after necking. With the transformation, the long period decreased gradually with increasing formation of new crystallite in the fibrils. These phenomena are agreed with the model proposed by Yamaguchi et al. [13].

As mentioned Section 3.4, the (001') diffraction was very weak and disappeared immediately after necking for fibers drawn at draw ratio 3.0 and 3.3. The draw ratio 3.0 is the minimum draw ratio, and it is almost the same with the NDR of as-spun fiber. Because the NDR is closely related to the yielding, intensity of the (001') diffraction indicates that the excessive drawing stress over the yielding stress is necessary to form the smectic phase. The excessive drawing stress aligns the molecular chains along the fiber axis, and bundles of the aligned molecular chains should form the smectic phase. In contrast, the shear-band-like structure was formed by the yielding stress at the minimum draw ratio, while it was not observed for the higher draw ratio. For the latter case, we think that a part of molecular bundle formed along the shear-band was aligned to the fiber axis by the excessive stress, and the smectic phase was formed at necking instead of the shear-band-like structure.

The draw ratio dependences of the drawn fiber properties, shown in Table 2, can be explained by the fiber structure development. For draw ratios of 3.0–4.2, the change in the properties can be explained by an increase in the amount of smectic phase. The larger amount of the highly oriented fibrillar smectic phase transformed into the larger amount of long-period structure consist of a sequence of crystallites and amorphous phases. Because the larger the amount of taut tie chains connecting the crystallites in the long period structure bears the more tensile force applied to the drawn fiber in tensile test, a higher Young's modulus, higher tensile strength, and larger shrinkage stress of the drawn fiber were obtained [2, 3]. With increasing draw ratio from 4.2–4.5, the amount of smectic phase did not change but its *d*-spacing increased. The larger *d*-spacing in the smectic phase and smaller tilting angle is caused by higher drawing stress, which should be applied to the fibrillar smectic phases and molecular network connecting them. Because the more tensile force is applied to the molecular network connecting fibrils, which is the weakest point of the structure, the tensile strength increases

more with increasing draw ratio. The molecular network connecting fibrils can be thought as the part of the stress-bearing network structure which determines the tensile strength of PET fibers [33].

DR 3.0

DR 4.2 - 4.5

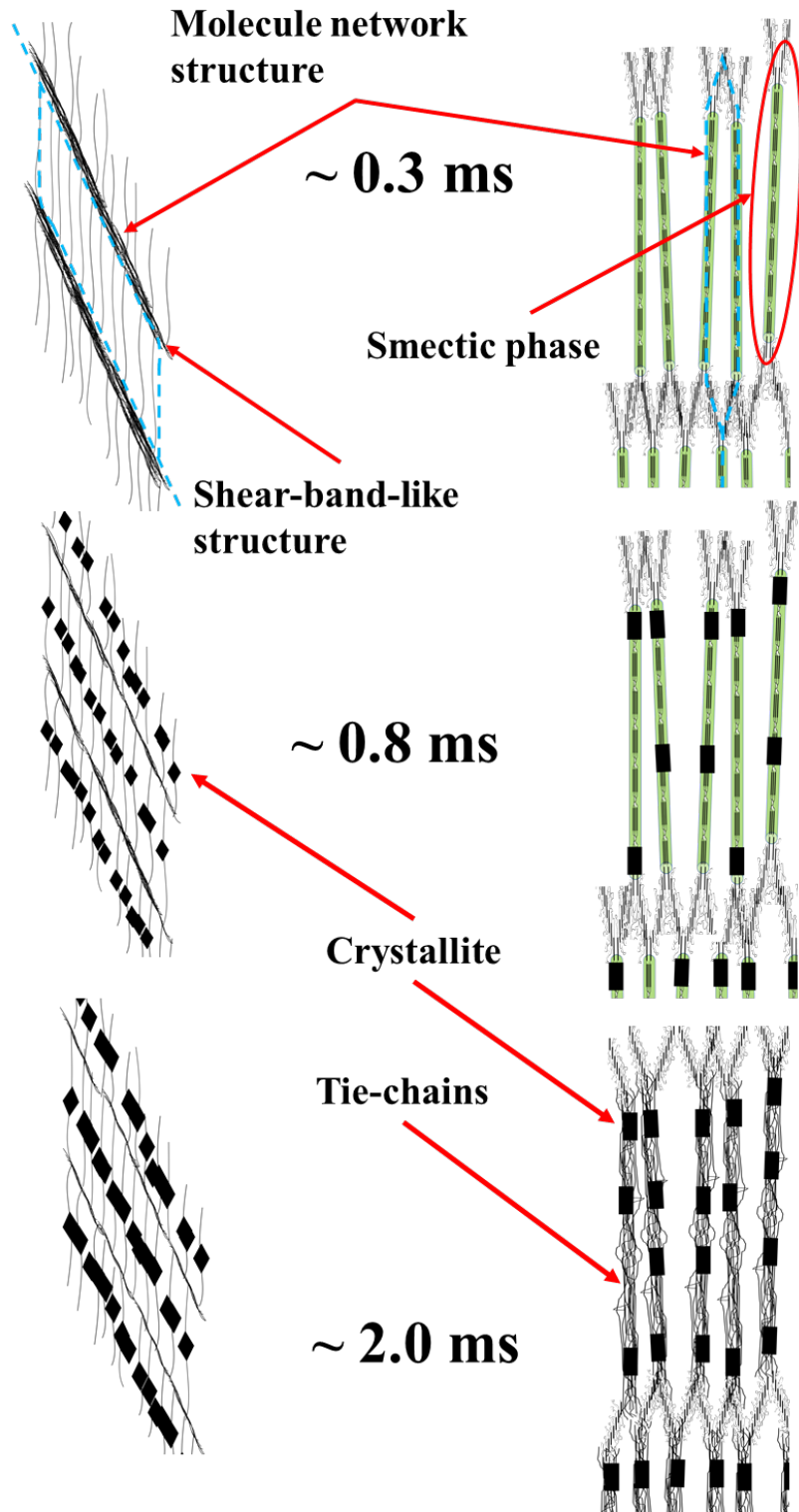


Figure 11 Schematic diagram of fiber structure development. The structures of the molecular network in the fiber are shown as blue lines.

4. Conclusion

We investigated the effects of draw ratio on the fiber structure development of PET during continuous neck-drawing at draw ratios from 3.0 to 4.5, or drawing stress from 22 to 149 MPa. The fiber structure development was investigated using simultaneous WAXD/SAXS measurements until 2.0 ms after necking with a time resolution of 0.09–0.16 ms, achieved using an ultrahigh-intensity X-ray beam generated by the SPring-8 synchrotron facility equipped with an undulator.

An X-shaped SAXS pattern was observed, but no (001') smectic phase diffraction was observed for the minimum stable draw ratio. The intensity of the (001') diffraction increased with increasing draw ratio up to 4.2. However, no clear draw ratio dependences of the crystallization rate and induction time, 2.3–2.8 ms⁻¹ and 0.4–0.6 ms, respectively, were observed. The *d*-spacing of the smectic (001') diffraction and the long period both clearly decreased within 1 ms after necking. They increased with increasing draw ratio up to 4.2, whereas the (001') *d*-spacing increased between draw ratios of 4.2 and 4.5.

The increase in the (001') intensity suggests that a larger amount of fibrillar structures consisting of molecular bundles was formed with increasing draw ratio up to 4.2, and the larger *d*-spacing for a draw ratio of 4.5 suggests that more constrained molecular bundles formed in the fibrillar structure. The larger amount of constrained fibrillar structures can bear a greater tensile force in tensile tests, therefore the drawn fibers have higher tensile strengths.

Acknowledgments

This study was supported by Grants-in-Aid for Scientific Research No. 23550240 and No. 16K05910 from the Education and Science Ministry, Japan. Experiments were performed at the SPring-8 synchrotron radiation facility, under application number 2013B7263.

References

- 1) J. R. Whinfield, J. T. Dickson, British Patent, 1941, 578 079 ICI.
- 2) B. K. Samui, M. P. Prakasan, C. Ramesh, D. Chakrabarty, R. Mukhopadhyay, *J. Textile Institute*, 104, (2013), 35-45.
- 3) Y. Liu, L. Yin, H. Zhao, G. Song, F. Tang, L. Wang, H. Shao, Y. Zhang, *J. Appl. Polym. Sci.*, 2015, DOI: 10.1002/APP. 42512.
- 4) H. Haberkorn, K. Hahn, H. Breuer, H.D. Dorrer, P. J Matthies, *J. Appl. Polym. Sci.*, 47, (1993), 1551-1579.
- 5) R. Kolb, S. Seifert, N. Stribeck, H.G. Zachmann, *Polymer*, 41, (2000), 2931-2935.
- 6) A. Mahendrasingam, C. Martin, W. Fuller, D. J. Blundell, R. J. Oldman, D. H. MacKerron, J. L. Harvie, C. Riekkel, *Polymer*, 41, (2000), 1217-1221.
- 7) D. Kawakami, B. S. Hsiao, C. Burger, S. Ran, C. Avila-Orta, I. Sics, T. Kikutani, B. Chu, *Macromolecules*, 38, (2005), 91-103.
- 8) S. Ran, X. Zong, D. Fang, B. S. Hsiao, B. Chu, R. Ross, *J. Appl Crystallogr.*, 33, (2000), 1031-1036.
- 9) J. Wu, J. M. Schultz, J. M. Samon, A. B. Pangelinan, H. H. Chuah, *Polymer*, 42, (2001), 7161-7170.
- 10) W. Okumura, T. Kanegae, Y. Ohkoshi, Y. Gotoh, M. Nagura, *Intern. Polym. Proc.*, 18, (2003), 46-52.
- 11) W. Okumura, T. Yamaguchi, Y. Ohkoshi, Y. Gotoh, M. Nagura, *Intern. Polym. Proc.*, 17, (2002), 124-132.
- 12) T. Yamaguchi, K. Komoriyama, Y. Ohkoshi, H. Urakawa, Y. Gotoh, N. Terasawa, M. Nagura, K. Kajiwara, *J. Polym. Sci., Polym. Phys.*, 43, (2005), 1090-1099.
- 13) T. Yamaguchi, K. H. Kim, T. Murata, M. Koide, S. Hitoosa, H. Urakawa, Y. Ohkoshi, Y. Gotoh, M. Nagura, M. Kotera, K. Kajiwara, *J. Polym. Sci., Polym. Phys.*, 46, (2008), 2126-2142.
- 14) K. H. Kim, T. Yamaguchi, Y. Ohkoshi, Y. Gotoh, M. Nagura, H. Urakawa, M. Kotera, T. Kikutani, *J. Polym. Sci., Polym. Phys.*, 47, (2009), 1653-1665.
- 15) K.H. Kim, T. Murata, Y.A. Kang, Y. Ohkoshi, Y. Gotoh, M. Nagura, H. Urakawa, *Macromolecules*, 44, (2011), 7378-7384.
- 16) K. H. Kim, R. Aida, Y. A. Kang, T. Ikaga, Y. Ohkoshi, I. Wataoka, H. Urakawa, *Polymer*, 53, (2012), 4272-4279.
- 17) Y. A. Kang, K. H. Kim, S. Ikehata, Y. Ohkoshi, Y. Gotoh, M. Nagura, M. Koide, H. Urakawa, *Polymer*, 52, (2011), 2044-2050.
- 18) K. Ide, T. Ikaga, Y. Ohkoshi, I. Wataoka, M. Masuda, Y. Maeda, *Sen'i Gakkaishi*, 70, (2014), 76-83.
- 19) K. H. Kim, Y.A. Kang, A. Yokoyama, T. Ikaga, Y. Ohkoshi, I. Wataoka, H. Urakawa, *Polymer*, 44,

- (2012), 1030-1035.
- 20) K. Sugawara, T. Ikaga, K.H. Kim, Y. Ohkoshi, K. Okada, H. Masunaga, T. Kanaya, M. Masuda, Y. Maeda, *Polymer*, 79, (2015), 37-46.
 - 21) A. Mehta, U. Gaur, B. Wunderlich, *J. Polym. Sci. Polym. Phys. Ed.*, 16, (1978), 289.
 - 22) S. Kase, T. Matsuo, *J. Polym. Sci., General Papers*, 3, (1965), 2541-2554.
 - 23) T. Asano, F. J. Balta Calleja, A. Flores, M. Tanigaki, M. Mina, C. Sawatari, H. Itagaki, H. Takahashi, I. Hatta, *Polymer*, 40, (1999), 6475-6484.
 - 24) R. Bonart, *Kolloid-Z*, 213, (1966), 1-11.
 - 25) T. Konishi, Y. Miyamoto, *Polymer*, 42, (2010), 349-353.
 - 26) Y. Y. Tomashpol'skii, G. S. Markova, *Polym. Sci. USSR*, 6, (1964), 316-324.
 - 27) H. Masunaga, H. Ogawa et. al., *Polym. J.* 43, 471-477 (2011).
 - 28) R. P. Daubeny, C. W. Bunn, *J. Polym. Sci., Polym. Chem.* 226, (1954), A1954, 531.
 - 29) J. Simizu, T. Kikutani, A. Takaku, N. Okui, *Sen'i Gakkaishi*, 40, (1984), T63-72.
 - 30) E. Funai, S. Sakurai, S. Hara, K. Yamamoto, S. Okamoto, J. Kojima, T. Kikutani, *Sen'i Gakkaishi*, 60, (2004), 322-330.
 - 31) K. Okada, M. Nakada, Y. Higashioji, K. Takahashi, Y. Ohkoshi, T. Kanaya, *Koubunshi Ronbunshu*, 71, (2014), 593-600.
 - 32) G. Stoclet, J.M. Lefebvre, R. Séguéla and C. Vanmansart, *Polymer*, 55, (2014), 1817-1828.
 - 33) T. Kikutani et al. "Fundamental and Practical Technologies for Nano-structured Polymeric Materials", 2008, p.56-110, CMC press, ISBN978-4-7813-0043-6.